

Tandem 3D-QSARs Approach as a Valuable Tool To Predict Binding Affinity Data: Design of New Gly/NMDA Receptor Antagonists as a Key Study

M. Bacilieri,[†] F. Varano,[‡] F. Deflorian,[†] M. Marini,[†] D. Catarzi,[‡] V. Colotta,[‡] G. Filacchioni,[‡]
A. Galli,[§] C. Costagli,[§] C. Kaseda,^{||} and S. Moro^{*,†}

Molecular Modeling Section, Department of Pharmaceutical Sciences, University of Padova, via Marzolo 5, I-35131 Padova, Italy, Dipartimento di Scienze Farmaceutiche, Università degli Studi di Firenze, Polo Scientifico, via Ugo Schiff, 6, 50019 Sesto Fiorentino (FI), Italy, Dipartimento di Farmacologia Preclinica e Clinica, Università degli Studi di Firenze, viale G. Pieraccini, 6, 50134 Firenze, Italy, and Yamatake Corporation, 1-12-2 Kawana, Fujisawa-shi Kanagawa, 251-8522 Japan

Received May 30, 2007

Quantitative structure–activity relationships (QSARs) represent a very well consolidated computational approach to correlate structural or property descriptors of chemical compounds with their chemical or biological activities. We have recently reported that autocorrelation Molecular Electrostatic Potential (autoMEP) vectors in combination to Partial Least-Square (PLS) analysis or to Response Surface Analysis (RSA) can represent an interesting alternative 3D-QSAR strategy. In the present paper, we would like to present how the applicability of in tandem linear and nonlinear 3D-QSAR methods (autoMEP/PLS&RSA) can help to predict binding affinity data of a new set of *N*-methyl-D-aspartate (Gly/NMDA) receptor antagonists.

INTRODUCTION

Quantitative structure–activity relationships (QSARs) represent a very well consolidated computational approach to correlate structural or property descriptors of chemical compounds with their chemical or biological activities.^{1–3} In particular, 3D-QSAR methods require the knowledge of the conformational properties of the molecules in order to calculate their structural or property descriptors. Comparative Fields Analysis (CoMFA) is probably one of the most successfully used 3D-QSAR methods in medicinal chemistry in the last two decades.⁴ Recently, we have reported that autocorrelation Molecular Electrostatic Potential (autoMEP) vectors in combination to Partial Least-Square (PLS) analysis can represent an alternative 3D-QSAR tool to CoMFA.^{5–8} Incidentally, both CoMFA and autoMEP/PLS methodologies can be classified as linear QSAR methods considering the mathematical relationship between molecular descriptors and chemical/biological response space. However, other QSAR strategies such as the artificial neural networks (ANN) or the support vector machines (SVM) are now widely applied in medicinal chemistry due to their ability to find a nonlinear relationship between descriptors and response space.^{9–14} Very recently, we have also presented a response surface analysis (RSA) application in tandem with the autoMEP descriptors (autoMEP/RSA) as an alternative nonlinear 3D-QSAR method.¹⁵

In the present paper, we would like to present how the applicability of in tandem linear and nonlinear 3D-QSAR methods (autoMEP/PLS&RSA) can help to predict binding affinity data of a new set of *N*-methyl-D-aspartate (NMDA) receptor antagonists.¹⁶ In particular, we would like to test the ability of our tandem autoMEP/PLS&RSA approach in discriminating “more active” vs “less active” analogs. This approach shares several analogies with the very well-known “consensus scoring” approach used in different molecular docking applications. According to this approach, multiple scoring functions are simultaneously used for model selection or virtual screening, and improvements can be achieved by compensating for the deficiencies of each function. Following this philosophy, we have proposed to simultaneously perform different 3D-QSAR approaches such as PLS and RSA, to create a more even balance between false positive and false negative performance rates than the use of a single method can achieve.¹⁵

The NMDA receptor together with α -amino-3-hydroxy-5-methyl-4-isoxazolepropionic acid (AMPA) and kainate (KA) receptors represents the most crucial class of transducers (ionotropic glutamate receptors, iGluRs) of the glutamatergic signaling circuits. The overactivation of iGluRs, especially of the NMDA receptor, seems to be involved in Parkinson, Huntington, and Alzheimer neurodegenerative disorders as well as in brain ischemia and epilepsy, because of the cell damage and death due to the overload of Ca^{2+} in cells.¹⁷ As a consequence, iGluRs antagonists represent an interesting potential therapeutic target, focusing in particular on the noncompetitive NMDA antagonists, which act at the glutamate coagonist glycine binding site on the NMDA receptor complex (Gly/NMDA).

In the recent past, our laboratory has been strongly involved in the elucidation of the structure–activity relation-

* Corresponding author phone: +39 049 827 5704; fax: +39 049 827 5366; e-mail: stefano.moro@unipd.it.

[†] University of Padova.

[‡] Dipartimento di Scienze Farmaceutiche, Università degli Studi di Firenze.

[§] Dipartimento di Farmacologia Preclinica e Clinica, Università degli Studi di Firenze.

^{||} Yamatake Corporation.

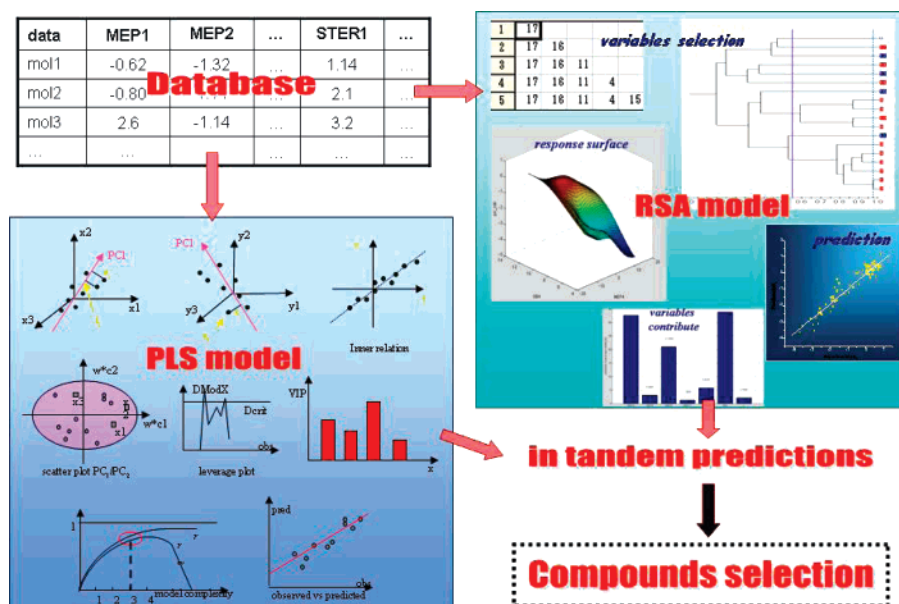


Figure 1. Flowchart of the PLS/RSA in tandem strategy for prediction of Gly/NMDA activity of new compounds.

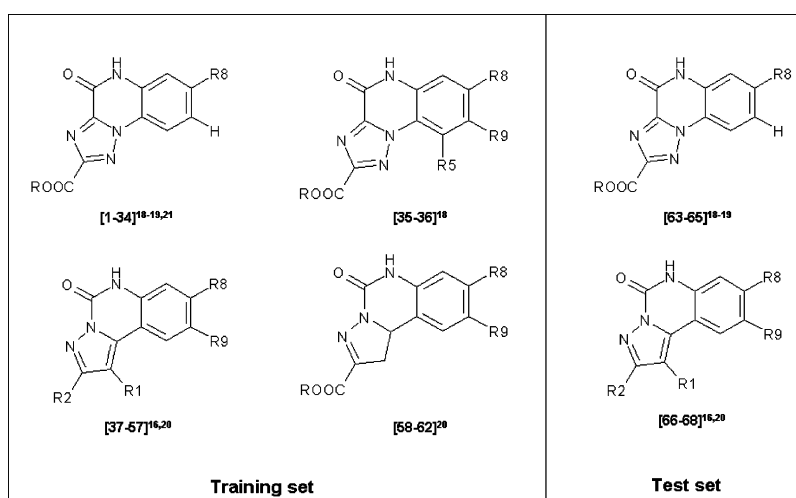


Figure 2. Structures of training and test set compounds.

ship of different chemical classes acting at Gly/NMDA, AMPA, and KA receptor antagonists.^{16,18-21}

The general flowchart of the PLS/RSA consensus strategy for prediction of Gly/NMDA receptor affinity of new compounds is reported in Figure 1.

MATERIALS AND METHODS

Computational Methodologies. All 3D-QSAR studies were carried out on a 8 CPU (PIV 2.0–3.0 GHZ) linux cluster running under openMosix architecture.²²

Autocorrelation MEP studies have been done using the ADRIANA (version 2.0) suite.²³ Partial Least-Square (PLS) analysis has been carried out using “The Unscrambler” statistical software.²⁴ Response Surface Analysis has been performed using DataForest and DataNesia software.^{25,26}

Molecular Structure Building. 3D models of all Gly/NMDA receptor antagonists (72 molecules) were obtained by using the 3D structure generator Corina. Corina is an integral part of the Adriana QSAR Suite.²³ Conformers generation and best conformer selection has been carried out using standard parameters of Corina. Conformer selection

is one of the most crucial steps in every 3D-QSAR approach. In this specific key study, due to the very limited conformational space for each Gly/NMDA antagonist, a very restricted number of conformers were generated. Moreover, following our previously reported docking studies, all selected conformers are conformationally coherent with the most energetically stable poses obtained from our docking studies. Protonation states are selected in agreement with the corresponding pK_a at the physiological pH value (7.4 unit).

Training Set. Throughout our previous published Gly/NMDA antagonists, we have selected as a training set for the computation of our models a collection of 62 compounds among 1,2,4-triazolo[1,5-*a*]quinoxaline-2-carboxylates (TQX) and pyrazolo[1,5-*c*]quinazoline-2-carboxylates (PQZ) derivatives^{16,18-21} (Figure 2).

Test Set. A test set of 6 molecules has been also selected for the validation process in the PLS/RSA models generation. Three compounds are 1,2,4-triazolo[1,5-*a*]quinoxaline-2-carboxylates (TQX) derivatives, and the other three molecules are pyrazolo[1,5-*c*]quinazoline-2-carboxylates (PQZ) derivatives^{16,18-21} (Figure 2).

Additional Test Set. A test set of 4 molecules has been finally proposed as an additional test set. The data set consists of 4 new synthesized antagonists: two new TQX and two PQZ analogues that have been designed based on our modeling studies.

Molecular Electrostatic Potential (MEP) Calculation.

In the present work MEPs derive from a classical point charge model: the electrostatic potential for each molecule is obtained by moving a unit positive point charge across the van der Waals surface, and it is calculated at various points j on this surface by the following equation

$$V_j = \sum_i^{\text{atoms}} \frac{q_i}{r_{ji}}$$

where q_i represents the partial charge of each atom i , and r_{ji} is the distance between points j and atom i .^{27–29} Starting from the 3D model of a molecule and its partial atomic charges, the electrostatic potential or another appropriate property is calculated for points on the molecular surface. Partial atomic charges were calculated by the PEOE method, and its extension to conjugated systems was implemented by the Petra module of the Adriana QSAR Suite.^{23,31,32} Connolly's solvent accessible surface with a solvent radius of 2.0 Å has been used to project the corresponding MEP. Once the autocorrelation function has been applied, the autocorrelation vector is obtained. Connolly's solvent accessible surface and the corresponding MEP have been calculated by the Surface module of the Adriana QSAR Suite.²³

Autocorrelation Vector. The first application of these vectors as molecular descriptors has been published by Moreau and Broto, who applied the classical mathematical notion of an autocorrelation function to the topology of molecular structures.^{32,33} The autocorrelation vector is presented as an intrinsic descriptor of the distribution of an atomic property along the molecular graph. Each component of the autocorrelation vector is calculated as follows

$$A(d) = \sum_{ij} p_i p_j$$

where A is the autocorrelation coefficient referring to atom pairs ij , p_i is the atomic property, and d is the ij topological distance.

Starting from this concept a new 3D descriptor has been introduced, based on the autocorrelation of properties at distinct points on the molecular surface.^{27–29} The different components of the autocorrelation vector are derived in this way

$$A(d_{\text{lower}}, d_{\text{upper}}) = 1/L \sum p_i p_j \quad (d_{\text{lower}} < d_{ij} < d_{\text{upper}})$$

where the ij distance d belongs to the d_{lower} , d_{upper} interval, and L is the number of distances in the same interval. The application of this concept made it possible to compare different molecular properties, as this 3D descriptor represents a compressed expression of the distribution of the property p on the molecular surface.^{27–29} The parameters for the calculation of the autocorrelation coefficient are the following: $d_{\text{lower}} = 1$ Å; $d_{\text{upper}} = 13$ Å; $L = 12$ point density = 10 points/Å²; and vdW radius reduction factor = 1.000. All parameters have been changed in various ways to see if it were possible to improve the model capability, but

nonsignificant results were derived. Considering distances from 1 to 13 Å, with a step width of 1 Å, 12 autocorrelation coefficients are calculated. This transformation produces a unique fingerprint of each molecule under consideration. Autocorrelation vectors have been calculated by the Surface module of the Adriana QSAR Suite.²³

Response Surface Analysis (RSA). For useful and predictive RSA models it is suggested to derive a model starting from a subset of the input x variables with the aim of reducing the dimensionality of the model itself.^{25,26,34–36} DataForest has been used for variables selections with the application in parallel of a linear stepwise regression and a nonlinear cluster analysis.²⁵ The basic concept of the stepwise regression is at first to add one at a time, in a linear regression manner, the variables x that best correlate with the response y and, second, to eliminate one at a time those x less correlated to the y from a regression equation containing initially all the independent variables. Final output reports the most important variables for the analysis. Second, the cluster analysis is performed, with the intent of dividing the data set into groups of molecules so that compounds in the same cluster are similar. The approach is based on a group average method, which uses the absolute value of the difference between 1 and the correlation coefficient among every variable as dissimilarity. The convergence of both methods guided us in the final choice of the subset of variables for the RSA model.^{25,26,36}

In the present work, the utilized RSA is based on a multivariate spline for interpolating the data.¹⁵ The equation of the thin plate spline algorithm that we applied is the following

$$y = \sum_{i=1}^n \alpha_i g(d_i) + \sum_{j=1}^p c_j x_j$$

where α_i and c_j represent the weight coefficients, p is the number of independent variables x , n is the number of data points, $g(d)$ is the Green's function, and d_i represents the Euclidean distance between data i and any x -coordinate. This algorithm can be explained regarding the response surface as the result of the calculation of an elastic beam displacement at the considered points (data), where the elastic beam has to be bended to reach the data points in the space. Consequently, the input values are regarded as points of force actions, while the output values are regarded as displaced values. RSA model computation has been derived on DataNesia software.²⁶

Sterimol Descriptors. Sterimol descriptors (L, B1, B2, B3, B4) have been calculated, using MOE suite, as originally proposed by Verloop and collaborators.^{37,38} Interestingly, Sterimol descriptors are intrinsically independent by translation and rotation motions of the molecule, and, consequently, they can be used together with autoMEP descriptors.

Structure-Based Molecular Modeling. As previously reported, the three-dimensional structures of iGluR extracellular binding domains were obtained from the Brookhaven Protein Data Bank (PDB). For docking, the structure of glycine-binding domain S1S2 of the NR1 subunit in complex with the antagonist DCKA (PDB code: 1PBQ) and the structure of glutamate-binding domain S1S2 of the GluR2 subunit in complex with the antagonist DNQX (PDB code:

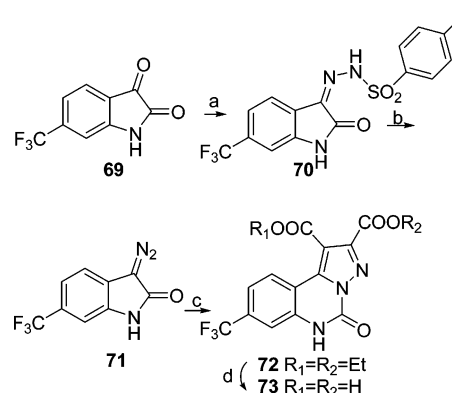
1FTL) were used.^{39,40} Since all X-ray crystallographic files do not contain hydrogen atoms, they need to be added to the protein by using the MOE modeling suite, before carrying out docking studies.³⁸ To minimize contacts between hydrogen atoms, the structures were subjected to AMBER94 energy minimization until the rms of conjugate gradient was $<0.15 \text{ kcal} \times \text{mol}^{-1} \times \text{\AA}^{-1}$, keeping the heavy atoms fixed at their crystallographic positions. All antagonist structures were generated by using the MOE suite.³⁸ Atomic charges were assigned using the PEOE, implemented by MOE. Each ligand was placed into the binding pockets, and the semi-flexible docking was achieved with the program Schrödinger/Glide.^{41–42} The final docked complexes of ligand–receptor were selected according to the criteria of interaction energy combined with geometrical matching quality.

Chemistry. Silica gel plates (Merck F254) were used for analytical chromatography. All melting points were determined on a Gallenkamp melting point apparatus. Microanalyses were performed with a Perkin-Elmer 260 elemental analyzer for C, H, and N, and the results were within $\pm 0.4\%$ of the theoretical values. The IR spectra were recorded with a Perkin-Elmer Spectrum RX I spectrometer in Nujol mulls and are expressed in cm^{-1} . The ^1H NMR spectra were obtained with a Varian Gemini 200. The chemical shifts are reported in δ (ppm) and are relative to the central peak of the solvent, which is always $\text{DMSO}-d_6$. All the exchangeable protons were confirmed by addition of D_2O . The following abbreviations are used: s = singlet, d = doublet, dd = double doublet, t = triplet, m = multiplet, br = broad, ar = aromatic protons (Schemes 1 and 2).

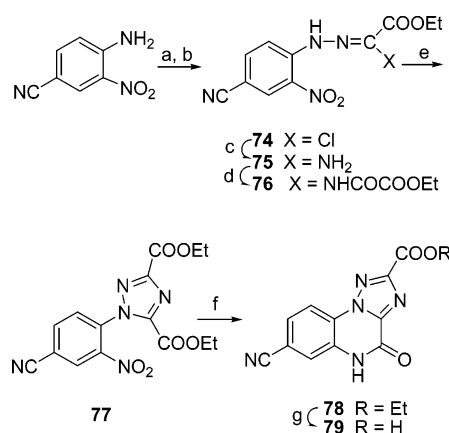
These new PQZ **72** and **73** and TQX derivatives **78** and **79** were synthesized as depicted in Schemes 1 and 2, respectively. Briefly, reaction of 6-trifluoromethyl isatine (**69**) with an equimolar amount of p-toluenesulfonylhydrazide gave the corresponding sulfonylhydrazone **70**, which, by hydrolysis in alkaline medium, led to 3-diazo-1,3-dihydroindol-2-one (**71**) (Scheme 1). The latter, after reaction with an excess of diethyl acetylene dicarboxylate, yielded the desired diethyl pyrazolo[1,5-c]quinazoline-1,2-dicarboxylate (**72**) that was easily hydrolyzed to the corresponding 1,2-dicarboxylic acid **73**.

The diazonium salt of commercially available 4-amino-3-nitrobenzonitrile was reacted with ethyl 2-chloro-3-oxobutanoate to yield the N^2 -chloroacetate **74**, which was transformed with ammonia into its corresponding N^2 -oxamidrazonate **75** (Scheme 2). By reacting **75** with ethyl oxalyl chloride, the N^3 -ethoxalyl derivative **76** was obtained, which was cyclized to the diethyl 1-(4-cyano-2-nitrophenyl)-1,2,4-triazole-3,5-dicarboxylate (**77**) by heating over its melting point. Reduction of the nitro group of **77** and contemporary cyclization directly afforded the tricyclic ester **78**, which was hydrolyzed to the corresponding 2-carboxylic acid **79**.

4-Methyl-N'-(6-trifluoromethyl-2-oxo-1,2-dihydro-3H-indol-3-ylidene)benzenesulfonylhydrazide (70). To a warmed (70°C) solution of isatine (**69**) (16 mmol) in methanol was added an equimolar amount of p-toluenesulfonylhydrazide (16 mmol).⁴³ The solution was allowed to stand at room temperature for 2 h, and then the resulting solid was collected by filtration and washed with a little cold methanol. Yield 80%. Mp 196°C dec (EtOH). ^1H NMR 2.36 (s, 3H, CH_3), 7.08–7.10 (m, 1H, ar), 7.35–7.45 (m, 3H, ar), 7.62 (d, 1H,

Scheme 1^a

^a Reagents: (a) p-toluenesulfonylhydrazide, MeOH, 80°C then room temperature; (b) 0.35 M NaOH, 60°C then room temperature; (c) diethyl acetylenedicarboxylate, anhydrous toluene, 110°C ; (d) 10% w/w KOH, EtOH, reflux.

Scheme 2^a

^a Reagent: (a) NaNO_2 /concentrated HCl, H_2O , 0°C ; (b) $\text{CH}_3\text{COCHClCOOEt}$, MeOH, room temperature; (c) NH_3 (gas), anhydrous dioxane, room temperature; (d) ClCOCOOEt , anhydrous diethyl ether, room temperature; anhydrous toluene, reflux; (e) neat, 160°C ; (f) iron powder, glacial AcOH, 90°C ; (g) 3% NaOH, EtOH, room temperature; 6 N HCl, 5°C .

ar, $J = 7.7$ Hz), 7.86 (d, 2H, ar, $J = 8.4$ Hz) 10.94 (br s, 1H, NH). Anal. ($\text{C}_{16}\text{H}_{12}\text{F}_3\text{N}_3\text{O}_3\text{S}$) C, H, N.

3-Diazo-6-trifluoromethyl-1,3-dihydro-indol-2-one (71). A suspension of **70** (4.3 mmol) in an aqueous solution of NaOH (0.35 M, 30 mL) was heated at 60°C for 1 h and then allowed to stand at room temperature for 2 h. Addition of ice (40 g) and acidification with acetic acid afforded a solid that was filtered and washed with water. The residue was unstable upon recrystallization. Nevertheless the crude product was pure enough and thus used without further purification. Yield 80%. ^1H NMR 7.11 (s, 1H, ar), 7.34 (d, 1H ar, $J = 8.0$ Hz), 7.63 (d, 1H, ar, $J = 8.0$ Hz), 10.97 (s, 1H, NH).

Diethyl 8-Trifluoromethyl-5,6-dihydro-5-oxo-pyrazolo[1,5-c]quinazoline-1,2-dicarboxylate (72). An excess of diethyl acetylene dicarboxylate (5.16 mmol) was added to a suspension of diazoindole **71** (2.58 mmol) in anhydrous toluene (50 mL). The resulting mixture was refluxed under nitrogen atmosphere for 5 h and then cooled at room temperature. The resulting solid was collected by filtration and washed with diethyl ether. Yield 70%. Mp $215\text{--}217^\circ\text{C}$ (EtOH). ^1H NMR 1.25–1.37 (m, 6H, 2 CH_3), 4.33–4.41 (m, 4H, 2 CH_2), 7.63–7.75 (m, 2H, ar), 8.72 (d, 1H,

ar, $J = 8.0$ Hz), 12.38 (br s, 1H, NH). Anal. ($C_{17}H_{14}F_3N_3O_5$) C, H, N.

8-Trifluoromethyl-5,6-dihydro-5-oxo-pyrazolo[1,5-*c*]-quinazoline-1,2-dicarboxylic Acid (73). An aqueous solution of KOH (10% w/w, 7 mL) was added to a suspension of diester **72** (0.8 mmol) in ethanol (7 mL). The mixture was heated at 100 °C for 1 h. Addition of water (15 mL) and acidification with concentrated HCl afforded a suspension that was heated at 100 °C for 1 h. After having been cooled to room temperature, the resulting solid was collected by filtration and well washed with water. Yield 70%. Mp > 300 °C (DMF/H₂O). ¹H NMR 7.66–7.72 (m, 2H, ar), 8.89 (d, 1H, ar, $J = 8.0$ Hz), 12.49 (s, 1H, NH). Anal. ($C_{13}H_6F_3N_3O_5$) C, H, N.

Ethyl N¹-(4-Cyano-2-nitrophenyl)hydrazono-N²-chloroacetate (74). Commercially available 4-amino-3-nitrobenzonitrile (18.37 mmol) was portionwise added to a solution of concentrated HCl (29 mL) and water (60 mL). The reaction mixture was kept at room temperature for one night and then cooled at 0 °C. A solution of NaNO₂ (5%, 10.8 mL) was dropwise added to the cooled (0 °C) mixture in an overall time of 30 min. After 20 min at 0 °C, the suspension was rapidly filtered under vacuum: the solid (unreacted 4-amino-3-nitrobenzonitrile) was reutilized, and the clear cold solution, containing the diazonium salt, was immediately used. A cold (0 °C) solution of ethyl 2-chloro-3-oxobutanoate (31.3 mmol) in methanol (30 mL) was added to the cold diazonium salt solution, which was kept at 0 °C for 10 min and then at room temperature for 3 h. The yellow solid which precipitated was collected by filtration and washed with cold methanol. Yield 60%. Mp 182–184 °C (EtOH). ¹H NMR 1.3 (t, 3H, CH₃, $J = 7.1$ Hz), 4.36 (q, 2H, CH₂, $J = 7.1$ Hz), 7.85 (d, 1H, ar, $J = 8.79$ Hz), 8.17 (dd, 1H, ar, $J = 8.79, 1.83$ Hz), 8.73 (d, 1H, ar, $J = 1.83$ Hz), 11.23 (br s, 1H, NH); IR 2230, 1726, 1530, 1376. Anal. ($C_{11}H_9ClN_4O_4$) C, H, N.

Ethyl N¹-(4-Cyano-2-nitrophenyl)-N²-oxamidrazonate (75). Ammonia was bubbled until saturation into a stirred solution of **74** (17.2 mmol) in anhydrous dioxane (100 mL). The mixture was stirred at room temperature until the disappearance of the starting material (TLC monitoring, eluting system CHCl₃) and then was diluted with water (200 mL) to yield a red solid, which was collected by filtration and washed with water. Yield 91%. Mp 173–175 °C (EtOH). ¹H NMR 1.28 (t, 3H, CH₃, $J = 7.11$ Hz), 4.27 (q, 2H, CH₂, $J = 7.11$ Hz), 7.02 (s, 2H, NH₂), 7.74 (d, 1H, ar, $J = 8.97$ Hz), 7.91 (d, 1H, ar, $J = 8.97$ Hz), 7.54 (s, 1H, ar), 10.22 (br s, 1H, NH); IR 3450, 3350, 2237, 1718, 1553, 1377. Anal. ($C_{11}H_{11}N_5O_4$) C, H, N.

Ethyl N¹-(4-Cyano-2-nitrophenyl)-N³-ethoxalylloxamidrazonate (76). A solution of ethylloxalyl chloride (26.3 mmol) in anhydrous diethyl ether (30 mL) was dropwise added to a suspension of the amidrazonate **75** (13.0 mmol) in anhydrous diethyl ether (100 mL). The addition was completed within 30 min, and, then, after addition of fresh anhydrous toluene (200 mL), the reaction mixture was heated at reflux for 1.5 h. After cooling at room temperature, a solid precipitated which was collected by filtration and washed with a little diethyl ether. A second crop of the desired product was obtained after evaporation at reduced pressure of the toluene solution: the solid residue was worked up with petroleum ether and collected by filtration. Yield 90%.

Mp 141–144 °C. ¹H NMR 1.25–1.32 (m, 6H, 2CH₃), 4.22–4.41 (m, 4H, 2CH₂), 7.87 (d, 1H, ar, $J = 8.79$ Hz), 8.13 (dd, 1H, ar, $J = 8.79, 1.47$ Hz), 8.67 (d, 1H, ar, $J = 1.47$ Hz), 11.01 (s, 1H, NH), 13.10 (s, 1H, NHCO); IR 3328, 2229, 1716, 1700, 1622, 1508, 1351. Anal. ($C_{15}H_{15}N_5O_7$) C, H, N.

Diethyl 1-(4-Cyano-2-nitrophenyl)-1,2,4-triazolo-3,5-dicarboxylate (77). Pure N³-ethoxalyl derivative **76** (1.3 mmol) was heated at 160 °C for 30 min. After having been cooled, the crude mass was dissolved in CHCl₃ (150 mL), and the resulting solution was washed with 0.5 N KOH (100 mL × 4) and then with water (100 mL × 2). After anidrification (Na₂SO₄), the organic layer was distilled under vacuum, and the resulting solid was worked up with a mixture of cyclohexane/ethyl acetate 1:1 and collected by filtration. Yield 53%. Mp 155–157 °C (CHX/AcOEt). ¹H NMR 1.18 (t, 3H, CH₃, $J = 7.14$ Hz), 1.33 (t, 3H, CH₃, $J = 7.11$ Hz), 4.27 (q, 2H, CH₂, $J = 7.14$ Hz), 4.40 (q, 2H, CH₂, $J = 7.11$ Hz), 8.17 (d, 1H, ar, $J = 8.43$ Hz), 8.54 (dd, 1H, ar, $J = 8.43, 1.83$), 8.96 (d, 1H, ar, $J = 1.83$). IR 2240, 1728, 1544, 1355. Anal. ($C_{15}H_{13}N_5O_6$) C, H, N.

Ethyl 7-Cyano-4,5-dihydro-4-oxo-1,2,4-triazolo[1,5-*a*]-quinoxaline-2-carboxylate (78). Iron powder (9.8 g) was added to a solution of **77** (9.8 mmol) in glacial acetic acid (50 mL). The mixture was heated at 90 °C for 30 min. Evaporation at reduced pressure of the solvent yielded a residue which was treated with water (25 mL) and then acidified with 6 N HCl. The solid was collected by filtration and extracted in Soxhlet with acetone (250 mL). Evaporation of the solvent at reduced pressure yielded a solid which was worked up with diethyl ether and filtered under vacuum. Yield 50%. Mp 287–288 °C. ¹H NMR 1.36 (t, 3H, CH₃, $J = 6.96$ Hz), 4.44 (q, 2H, CH₂, $J = 6.96$ Hz), 7.78 (s, 1H, ar), 7.80 (d, 1H, ar, $J = 8.42$ Hz), 8.27 (d, 1H, ar, $J = 8.42$ Hz), 12.53 (br s, 1H, NH); IR 3504, 2236, 1714, 1690. Anal. ($C_{13}H_9N_5O_3$) C, H, N.

7-Cyano-4,5-dihydro-4-oxo-1,2,4-triazolo[1,5-*a*]quinoxaline-2-carboxylic Acid (79). A solution of NaOH (3%, 19 mL) was added to a suspension of **78** (0.71 mmol) in EtOH (19 mL). The mixture was stirred at room temperature for 15 min. The solid was collected by filtration and resuspended in the minimal amount of water (20 mL); after acidification of the cold (5 °C) suspension by 6 N HCl, and standing 30 min in a ice bath, the resulting solid was collected by filtration and washed with water. Yield 83%. Mp > 300 °C. ¹H NMR 7.78 (s, 1H, ar), 7.80 (d, 1H, ar, $J = 8.06$ Hz), 8.25 (d, 1H, ar, $J = 8.06$), 12.68 (s, 1H, NH); IR 3240, 2231, 1710, 1680. Anal. ($C_{11}H_5N_5O_3$) C, H, N.

Binding Assay. Rat cortical synaptic membrane preparation and [³H]glycine, [³H]AMPA, and high-affinity [³H]-kainate binding experiments were performed, following the procedures already described in our previous papers.^{44–47} Table 1 reports the binding data for the new derivatives of the additional test set. For binding data of the training and test sets see the Supporting Information.

RESULTS AND DISCUSSION

Topological and electrostatic complementarities are two key concepts in the molecular recognition process. Gasteiger and collaborators investigated the MEP on a molecular surface as a particularly useful method for rationalizing the

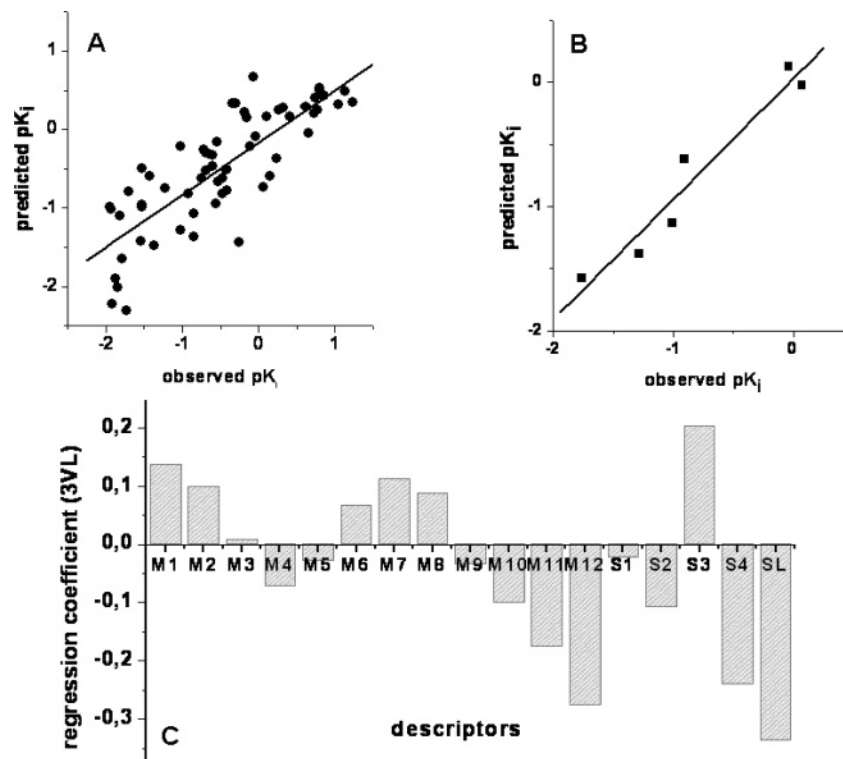


Figure 3. Summary of PLS statistics: (A) experimental vs predicted pK_i (after cross-validation) values corresponding to the training set; (B) experimental vs predicted pK_i values corresponding to the test set; and (C) regression weights for each descriptor in the final 3VL-PLS model.

Table 1. Displacement of [3H]glycine Binding^a

72-73		78-79			
no.	R ₁	R ₂	R ₇	R ₈	K_i (μM) [3H]glycine ^b
72	COOEt	COOEt	—	CF ₃	3.2 ± 0.3
73	COOH	COOH	—	CF ₃	0.072 ± 0.01
78	—	COOEt	CN	—	22 ± 4
79	—	COOH	CN	—	2.2 ± 0.3

^a The tested compounds were dissolved in 50% DMSO and then diluted with the appropriate buffer. ^b Inhibition constant (K_i) values were means \pm SEM of three or four separate determinations in triplicate.

interactions between molecules and molecular recognition processes.^{27–29} Indeed, values and spatial distribution of MEP might strongly influence the binding of a ligand to its active site. Obviously, MEPs property values as well as other molecular properties strongly depend on the spatial orientation of the different molecules. It has been already demonstrated that the introduction of the autocorrelation vector allows for overcoming the MEP information inconvenience to be reliant on the spatial rotation and translation of the molecule.^{27–29} In fact, autocorrelation vector descriptors represent a chemical structure with a vector of fixed length independent of the size of the molecule. Since only internal coordinates (topological or spatial distances of atom pairs or pairs of points on the molecular surface) are taken into account, the resulting descriptors are also independent from the orientation of the molecules in space (translation and

Table 2. Summary of PLS Statistics

mol set	62
principal components	3
r	0.81
r_{cv} ^a	0.75
q	0.97
slope	0.66
offset	−0.16
RMSEC ^b	0.52
RMSEP ^c	0.59
SEC ^d	0.52
SEP ^e	0.60
bias ^f	−5 ^{−8}

^a Cross-validated r after leave-one-out procedure: $r_{cv} = [(SD - PRESS)/SD]^{1/2}$, $SD = (Y_{actual} - Y_{mean})^2$, and $PRESS = \sum (Y_{predicted} - Y_{actual})$. ^b RMSEC – root mean squares of calibration. ^c RMSEP – root mean squares of prediction. ^d SEC – standard error of calibration. ^e SEP – standard error of prediction. ^f Bias – systematic difference between predicted and observed values.

rotation invariant). On the other hand, topological descriptors, such as Sterimol descriptors, are able to characterize structures according to their size, conformation, and overall shape. As described by Verloop and collaborators, Sterimol descriptors are intrinsically invariant to translation and rotation.³⁷ Therefore, the combined use of both autoMEP and Sterimol descriptors might help to appropriately address the topological and the electrostatic properties of a ligand considering this hybrid autoMEP-Sterimol vector as a sort of interaction fingerprint of each ligand conformer.

In this work, using our hybrid autoMEP-Sterimol vectors, we have verified the possibility of combining two different linear and nonlinear 3D-QSAR strategies, such as PLS and RSA, to prioritize the synthesis of new ligands (Figure 1).

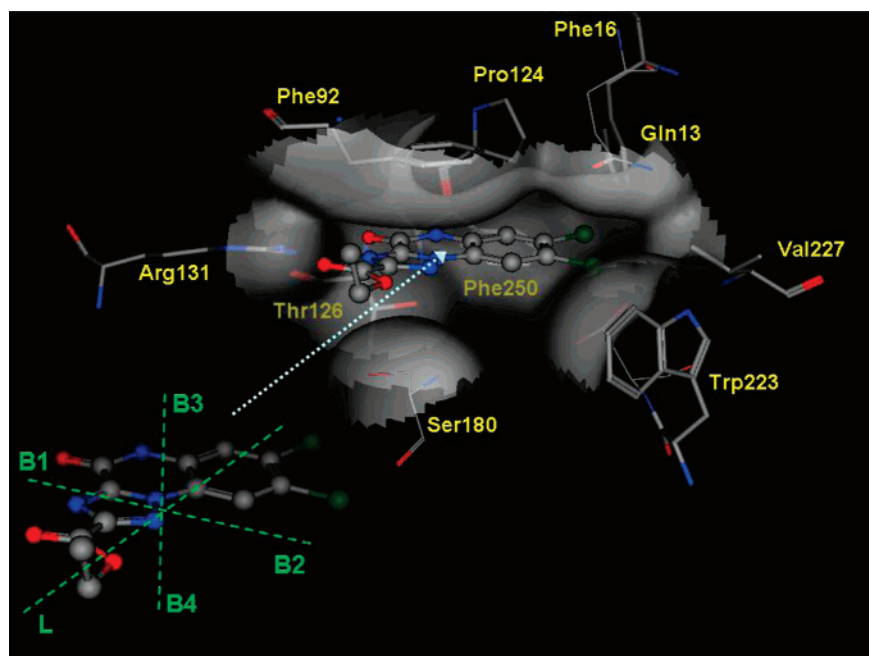


Figure 4. Representation of the Sterimol descriptors of a Gly/NMDA receptor antagonist in the active site of the target.

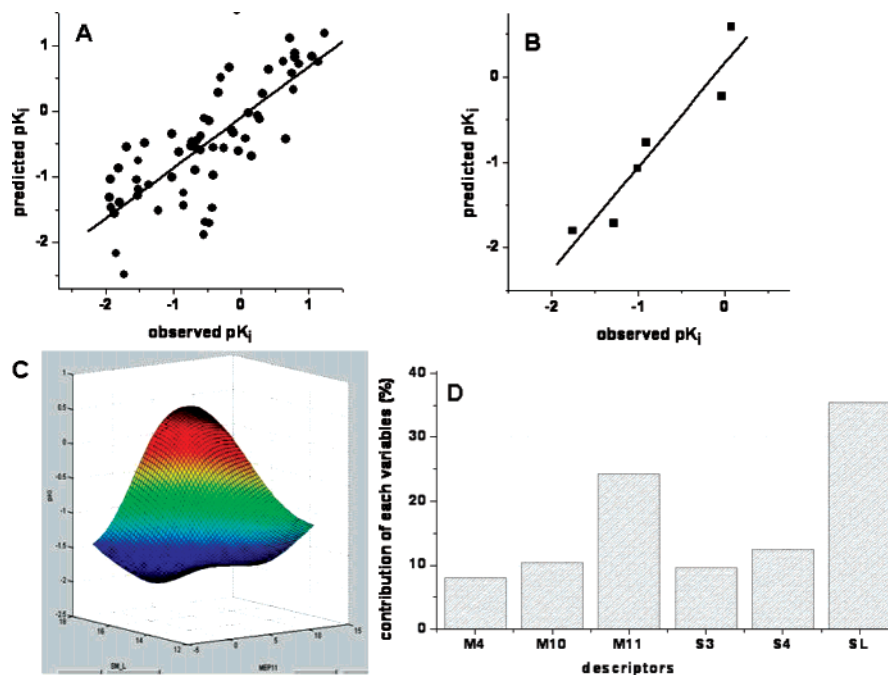


Figure 5. Summary of RSA statistics: (A) experimental vs predicted pK_i (after cross-validation) values corresponding to the training set; (B) experimental vs predicted pK_i values corresponding to the test set; (C) representation of response surface obtained by plotting pK_i vs MEP11 and SL, maintaining constant the other descriptors values; and (D) contribution in % of each descriptor in the final RSA model.

Starting from our previous published Gly/NMDA receptor antagonists, we have selected a collection of 62 derivatives among 1,2,4-triazolo[1,5-*a*]quinoxaline-2-carboxylates (TQX) and pyrazolo[1,5-*c*]quinazoline-2-carboxylates (PQZ) derivatives.^{16,18–21} Moreover, a test set of 6 molecules has been also utilized in the model validation process (Figure 2).

As anticipated, PLS analysis has been performed using 17 molecular descriptors (12 autoMEP and 5 Sterimol descriptors) derived for each compound. The resulting model has shown good statistical quality in both calibration and internal validation steps as demonstrated by the r and r_{cv} values of 0.81 and 0.75, respectively, using only three latent variables (Figure 3 and Table 2).

Analyzing the contribution of each descriptors on the three latent variables, we found that both steric and electrostatic effects are equally crucial in affecting ligand–receptor binding affinity. Interestingly, Sterimol descriptors L, B3, and B4 are nicely compatible with the Gly/NMDA receptor-driven pharmacophore model recently published by our group. In fact, starting from the docking pose obtained for these two classes of Gly/NMDA receptor antagonists, we verified that all critical Sterimol descriptors can describe the steric control observed in positions R2 and R8 using sterically hindered substituents as shown in Figure 4.

The robustness of the abovementioned PLS model is also supported by the high value of the correlation co-

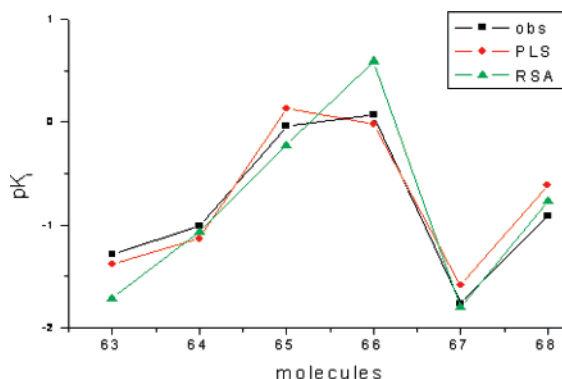


Figure 6. Test set predictions and PLS/RSA results comparison.

Table 3. Summary of RSA Statistics

mol set	62
variables	6
r	0.99
r_{cv}^a	0.77
q	0.95
slope	0.77
offset	-0.09
RSS ^b	2.37

^a Cross-validated r after leave-one-out procedure: $r_{cv} = [(SD - PRESS)/SD]^{1/2}$, $SD = (Y_{actual} - Y_{mean})^2$, and $PRESS = \sum (Y_{predicted} - Y_{actual})$.

^b RSS – residual sum of squares.

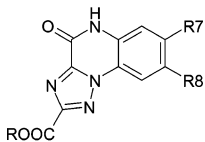
efficient calculated on the test set ($q = 0.97$) (Figure 3 and Table 2).

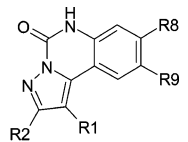
In parallel, we have delivered a nonlinear RSA model using the same training and test data sets. The stepwise regression analysis together with the cluster analysis on the original 17 molecular descriptors led us to select six of them as a final better combination to utilize as independent variables for the RSA model: the autoMEP 4, 10, and 11 and the Sterimol B3, B4, and L. We can notice that these descriptors are recognized as essentially even in PLS analysis (Figure 3). The statistical parameters and the final RSA model are collected in Figure 5 and Table 3.

We can notice the very high correlation coefficient ($r = 0.99$) value for the calibration step confirming the good choice of the independent variables selection. The correlation coefficient for the test set is also appreciable ($r_{cv} = 0.77$) as in the case of PLS prediction. Both methods are acceptably accurate in the prediction of the test set. Even if RSA predictivity is slightly less accurate than PLS (see derivatives **63** and **66** in Figure 6 and Table 4), both methodologies coherently discriminate between “more active” and “less active” analogs.

Following these encouraging results, we tested the real predictive capability of our PLS&RSA models on an additional test set, which consisted of 4 new synthesized antagonists, two new TQX and two PQZ analogues that have been designed based on our modeling studies. In particular, in the new TQX derivatives, a nitrile group was introduced at the R7 position in both acid and ethyl ester scaffolds. On the contrary, a CF₃ group at the R8 position was introduced in PQZ scaffolds as reported in Table 5. Even if we are aware about the limited number of compounds selected in this preliminary additional test set, we would like to utilize it as a preliminary proof of concept of our tandem PLS&RSA approach. As anticipated in the Introduction, the main goal

Table 4.





ID	observed p <i>K</i> _i	PLS p <i>K</i> _i	RSA p <i>K</i> _i	PLS residuals	RSA residuals
63	-1.28	-1.38	-1.71	0.10	0.43
64	-1.01	-1.13	-1.07	0.12	0.06
65	-0.04	0.13	-0.23	-0.17	0.19
66	0.07	-0.02	0.59	0.09	-0.52
67	-1.76	-1.58	-1.80	-0.17	0.04
68	-0.91	-0.62	-0.77	-0.30	-0.14

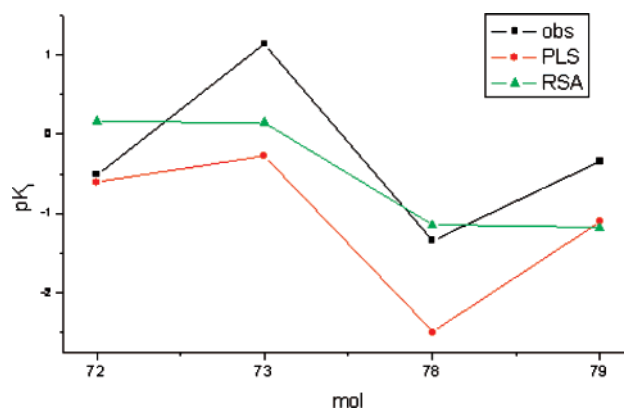
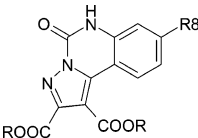
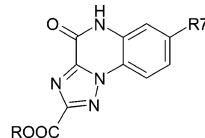


Figure 7. Additional test set predictions with the in tandem method.

Table 5.

	
72 R=Et R8=CF ₃	78 R=Et R7=CN
73 R=H R8=CF ₃	79 R=H R7=CN

ID	observed pK _i	PLS pK _i	RSA pK _i	PLS residuals	RSA residuals
72	-0.51	-0.61	0.16	0.10	-0.67
73	1.14	-0.27	0.15	1.41	0.99
78	-1.34	-2.50	-1.14	1.16	-0.20
79	-0.34	-1.10	-1.19	0.76	0.85

of simultaneously performing different 3D-QSAR approaches, such as PLS and RSA, is the possibility of creating a more even balance between false positive and false negative performance rates than use of a single method can achieve.

Once molecular descriptors have been computed for this set of molecules we have passed the data through the two models for predictions. Looking at the pK_i values we can see that the trend of both models predictions is the same, except for the molecule **78** for which there is a difference of just a bit more than a log unit between the two predicted activity values (Figure 7 and Table 5). Our idea is to apply this approach for screening of libraries of new optimized compounds. In this context, using in tandem the PLS and RSA models should make us select only the compounds that have been predicted with a high activity in both cases (in this specific case ± 1.5 pK_i units) and, consequently, to derive

experimentally only the more interesting and optimized molecules.

The experimental data for the four molecules were obtained in a second step. The observed pK_i values have confirmed the usefulness of our in tandem strategy application for the optimization of new proposals. In fact, we can see that if we should have made a selection of the most actives only based on the PLS model prediction (the one with the best predictive performance based on our training set, see Figure 4) we should have failed to correctly predict compound **78**, overestimating its activity as a Gly/NMDA receptor antagonist. Interestingly, on the contrary with respect to the training set, in this additional test set we can observe that the RSA predictivity is slightly better than PLS, supporting our initial feeling concerning the applicability of the in tandem strategy as a useful tool as the pK_i predictor.

We want to remind the reader, finally, that the screening application of these kinds of strategies is aimed to select new compounds not in an exactly quantitative manner but in a qualitative mode, so to select compounds that effectively prove to be promising when we have designed libraries of possible new molecules.

CONCLUSIONS

In our paper the application of two different, linear and nonlinear correlations, QSAR methodologies in tandem with a receptor-based drug strategy has been thoroughly described to suggest their introduction as parallel tools in a generic 3D-QSAR analysis. Statistically meaningful models have been generated from a common training set, and promising results concerning Gly/NMDA antagonists have been highlighted by their comparison and by the binding affinity prediction on the test sets. In addition, the combination of PLS and RSA with autoMEP and Sterimol molecular descriptors seems to be effective in rationalizing information coming from the analyzed compounds in three-dimensional space. We propose this parallel strategy for the development of alternative calibrations with other databases. The purpose is to perform in silico screening of real or virtual libraries to search diverse interesting structures with significant biological activity by applying both approaches.

ACKNOWLEDGMENT

We thank the Molecular Network GmbH (Erlangen, Germany) for the assistance in using the ADRIANA modeling suite. The molecular modeling work coordinated by S.M. has been carried out with financial support from the Italian Ministry for University and Research (MIUR), Rome, Italy and from the University of Padova, Padova, Italy. S.M. is also very grateful to the Chemical Computing Group for the scientific and technical partnership.

Supporting Information Available: Information concerning the experimental details. This material is available free of charge via the Internet at <http://pubs.acs.org>.

REFERENCES AND NOTES

- Hansch, C.; Leo, A. Exploring QSAR. In *Fundamentals and Applications in Chemistry and Biology*; American Chemical Society: Washington, DC, U.S.A., 1995.
- Bacilieri, M.; Moro, S. Ligand-based drug design methodologies in drug discovery process: an overview. *Curr. Drug Discovery Technol.* **2006**, *3*, 155–165.
- Moro, S.; Bacilieri, M.; Deflorian, F. Combining ligand-based and structure-based drug design in the virtual screening arena. *Expert Opin. Drug Discovery* **2007**, *2*, 37–49.
- Cramer, R. D.; Patterson, D. E.; Bunce, J. D. Comparative Molecular Field Analysis (CoMFA). 1. Effect of shape on binding of steroids to carrier proteins. *J. Am. Chem. Soc.* **1988**, *110*, 5959–5967.
- Wold, S.; Sjostrom, M.; Eriksson, L. Partial Least Squares Projections to Latent Structures (PLS) in chemistry. In *The encyclopaedia of computational chemistry*; Schleyer, P. v. R., Ed.; John Wiley & Sons: New York, U.S.A., 2006; p 2022.
- Moro, S.; Bacilieri, M.; Ferrari, C.; Spalluto, G. Autocorrelation of molecular electrostatic potential surface properties combined with Partial Least Squares analysis as alternative attractive tool to generate ligand-based 3D-QSARs. *Curr. Drug Discovery Technol.* **2005**, *2*, 13–21.
- Moro, S.; Bacilieri, M.; Cacciari, B.; Spalluto, G. Autocorrelation of molecular electrostatic potential surface properties combined with partial least squares analysis as new strategy for the prediction of the activity of human A_3 adenosine receptor antagonists. *J. Med. Chem.* **2005**, *48*, 5698–704.
- Moro, S.; Bacilieri, M.; Cacciari, B.; Klotz, K. N.; Spalluto, G. The application of a 3D-QSAR (autoMEP/PLS) approach as an efficient pharmacodynamic-driven filtering method for small-size virtual library: application to a lead optimization of a human A_3 adenosine receptor antagonist. *Bioorg. Med. Chem.* **2006**, *14*, 4923–4932.
- Moro, S.; Bacilieri, M.; Deflorian, F. Combining ligand-based and structure-based drug design in the virtual screening arena. *Expert Opin. Drug Discovery* **2007**, *2*, 1–13.
- Zupan, J.; Gasteiger, J. *Neural networks in chemistry and drug design*, 2nd ed.; Wiley-VCH: Weinheim, Germany, 1999.
- Gasteiger, J.; Teckentrup, A.; Terfloth, L.; Spycher, S. Neural Networks as Data Mining Tools in drug design. *J. Phys. Org. Chem.* **2003**, *16*, 232–245.
- Czerminski, R.; Yarsi, A.; Hartsough, D. Use of Support Vector Machine in pattern classification: application to QSAR studies. *QSAR* **2001**, *20*, 227–240.
- Norinder, U. Support Vector Machine models in drug design: applications to drug transport processes and QSAR using simplex optimisations and variable selection. *Neurocomputing* **2003**, *55*, 337–346.
- Warmuth, M.; Liao, J.; Ratsch, G.; Mathieson, M.; Putta, S.; Lammen, C. Active learning with Support Vector Machines in the drug discovery process. *J. Chem. Comput. Sci.* **2003**, *43*, 667–673.
- Bacilieri, M.; Kaseda, C.; Spalluto, G.; Moro, S. Response surface analysis as alternative 3D-QSAR tool: human A_3 adenosine receptor antagonists as key study. *Lett. Drug Des. Disc.* **2007**, *4*, 122–127.
- Varano, F.; Catarzi, D.; Colotta, V.; Calabri, F. R.; Lenzi, O.; Filacchioni, G.; Galli, A.; Costagli, C.; Deflorian, F.; Moro, S. 1-Substituted pyrazolo[1,5-c]quinazolines as novel Gly/NMDA receptor antagonists: synthesis, biological evaluation and molecular modeling study. *Bioorg. Med. Chem.* **2005**, *13*, 5536–5549.
- Brauner-Osborne, H.; Egebjerg, J.; Nielsen, E. O.; Madsen, U.; Krosgaard-Larsen, P. Ligands for glutamate receptors: design and therapeutic prospects. *J. Med. Chem.* **2000**, *43*, 2609–2645.
- Catarzi, D.; Colotta, V.; Varano, F.; Cecchi, L.; Filacchioni, G.; Galli, A.; Costagli, C. 45-Dihydro-124-triazolo[15-a]quinoxaline-2-ones: excitatory amino acid antagonists with combined glycine/NMDA and AMPA receptor affinity. *J. Med. Chem.* **1999**, *42*, 2478–2484.
- Catarzi, D.; Colotta, V.; Varano, F.; Filacchioni, G.; Galli, A.; Costagli, C.; Carla, V. Synthesis ionotropic glutamate receptor binding affinity and structure-activity relationships of a new set of 45-dihydro-8-heteroaryl-4-oxo-124-triazolo[15-a]quinoxaline-2-carboxylates analogues of TQX-173. *J. Med. Chem.* **2001**, *44*, 3157–3165.
- Varano, F.; Catarzi, D.; Colotta, V.; Filacchioni, G.; Galli, A.; Costagli, C.; Carla, V. Synthesis and biological evaluation of a new set of pyrazolo[1,5-c]quinazoline-2-carboxylates as novel excitatory amino acid antagonists. *J. Med. Chem.* **2002**, *45*, 1035–1044.
- Catarzi, D.; Colotta, V.; Varano, F.; Calabri, F. R.; Filacchioni, G.; Galli, A.; Costagli, C.; Carla, V. Synthesis and biological evaluation of analogues of 7-chloro-45-dihydro-4-oxo-8-(124-triazol-4-yl)-124-triazolo[15-a]quinoxaline-2-carboxylic acid (TQX-173) as novel selective AMPA receptor antagonists. *J. Med. Chem.* **2004**, *47*, 262–272.
- Bar, M. *OpenMosix, version 2.4.26*; Tel Aviv University: Tel Aviv, Israel, 2004.
- Adriana, version 2.0; Molecular Networks GmbH: Erlangen, Germany, 2003.
- The Unscrambler, version 9.2; CAMO Process AS: Oslo, Norway, 2003.
- DataFOREST, version 9; Yamatake Corporation: Fujisawa-shi Kanagawa, Japan, 2007.
- DataNESIA, version 3.2; Yamatake Corporation: Fujisawa-shi Kanagawa, Japan, 2007.

- (27) Gasteiger, J.; Li, X.; Rudolph, C.; Sadovski, J.; Zupan, J. Representation of Molecular Electrostatic Potential by topological feature maps. *J. Am. Chem. Soc.* **1994**, *116*, 4608–4620.
- (28) Wagener, M.; Sadovski, J.; Gasteiger, J. Autocorrelation of molecular surface properties for modeling corticosteroid binding globulin and cytosolic Ah receptor activity by neural networks. *J. Am. Chem. Soc.* **1995**, *117*, 7769–7778.
- (29) Bauknecht, H.; Zell, A.; Bayer, H.; Levi, P.; Wagener, M.; Sadowski, J.; Gasteiger, J. Locating biologically active compounds in medium-sized heterogeneous data sets by topological autocorrelation vectors: dopamine and benzodiazepine agonists. *J. Chem. Inf. Comput. Sci.* **1996**, *36*, 1205–13.
- (30) Gasteiger, J.; Marsili, M. Iterative Partial Equalization of Orbital Electronegativity - A rapid access to atomic charges. *Tetrahedron* **1980**, *36*, 3219–3228.
- (31) Gasteiger, J.; Saller, H. Berechnung der Ladungsverteilung in konjugierten Systemen durch eine Quantifizierung des Mesomeriekonzeptes. *Angew. Chem.* **1985**, *97*, 699–701.
- (32) Moreau, G.; Broto, P. The autocorrelation of a topological structure: a new molecular descriptor. *Nouv. J. Chim.* **1980**, *4*, 359–360.
- (33) Moreau, G.; Broto, P. Autocorrelation of molecular structures, application to SAR studies. *Nouv. J. Chim.* **1980**, *4*, 757–764.
- (34) Myers, R.; Montgomery, D. C. *Response methodology surface*; John Wiley, Ed.; Wiley-Interscience: New York, U.S.A., 1995.
- (35) Amago, T. Sizing optimisation using response surface method in FOA. *R&D Rev. Toyota* **37**, 1–7.
- (36) Kaseda, C. *Response Surface Methodology using a spline algorithm*; G.d.a.c.S., Ed.; Nashboro Press: Fujisawa-shi Kanagawa, Japan, 2004.
- (37) Verloop, A. *The sterinol approach to drug design*; Marcel Dekker: New York, U.S.A., 1987.
- (38) *Molecular Operating Environment, version 2006.08*; Chemical Computing Group: Montreal, Canada, 2006.
- (39) Furukawa, H.; Gouaux, E. Mechanisms of activation, inhibition and specificity: crystal structures of the NMDA receptor NR1 ligand-binding core. *EMBO J.* **2003**, *22*, 2873–2885.
- (40) Armstrong, N.; Gouaux, E. Mechanisms for activation and antagonism of an AMPA-sensitive glutamate receptor: crystal structures of the GluR2 ligand binding core. *Neuron* **2000**, *28*, 165–182.
- (41) Friesner, R. A. Glide. A new approach for rapid, accurate docking and scoring. 1. Method and assessment of docking accuracy. *J. Med. Chem.* **2004**, *47*, 1739–1749.
- (42) Halgren, T. A. Glide: A new approach for rapid, accurate docking and scoring. 2. Enrichment factors in database screening. *J. Med. Chem.* **2004**, *47*, 1750–1759.
- (43) Hewawasam, P.; Meanwell, N. A. A general method for the synthesis of isatins: preparation of regiospecifically functionalized isatins from anilines. *Tetrahedron Lett.* **1994**, *40*, 7303–7306.
- (44) Varano, F.; Catarzi, D.; Colotta, V.; Cecchi, L.; Filacchioni, G.; Galli, A.; Costagli, C. Synthesis of a set of ethyl 1-carbamoyl-3-oxoquinoline-2-carboxylates and of their constrained analogue Imidazo-[1,5-a]quinoxaline-1,3,4-triones as selective Glycine/NMDA receptor antagonists. *Eur. J. Med. Chem.* **2001**, *36*, 203–209.
- (45) Varano, F.; Catarzi, D.; Colotta, V.; Filacchioni, G.; Galli, A.; Costagli, C.; Carla, V. Synthesis and biological evaluation of a new set of Pyrazolo[1,5-c]quinazoline-2-carboxylates as novel excitatory amino acid antagonists. *J. Med. Chem.* **2002**, *45*, 1035–1044.
- (46) Colotta, V.; Catarzi, D.; Varano, F.; Cecchi, L.; Filacchioni, G.; Galli, A.; Costagli, C. Synthesis and biological evaluation of a series of quinazoline-2-carboxylic acids and quinazoline-2,4-diones as Glycine-NMDA antagonists: a pharmacophore model based approach. *Arch. Pharm. Pharm.* **1997**, *330*, 129–134.
- (47) Nielsen, E. O.; Madsen, U.; Schaumburg, K.; Brehm, L.; Krogsgaard-Larsen, P. Studies on receptor-active conformations of excitatory amino acid agonists and antagonists. *Eur. J. Med. Chem.* **1986**, *21*, 433–445.

CI7001846